Final Report

NCPTT 2016 Grants
Award P16AP00359

3D Analysis and Visualization of Tideline Changes to Cellulosic Structures

PI: Rachel Obbard PhD, Dartmouth College

Rachel Obbard (rachel.w.obbard@dartmouth.edu)
Lynn Brostoff, PhD, Library of Congress (LC)
Silvia A. Centeno, PhD, Metropolitan Museum of Art (MMA)

December 15, 2017

Table of Contents

1. INTRODUCTION 4

2. MATERIALS AND METHODS 5
   2.1 Sample Selection 5
   2.2 X-ray fluorescence (XRF) 7
   2.3 Synchrotron XRF (SXRF) 8
   2.4 Scanning electron microscopy-energy dispersive X-ray spectroscopy (SEM-EDS) 8
   2.5 X-ray micro computed tomography (microCT) 8
   2.6 Tensile Testing 9

3. RESULTS AND DISCUSSION 10
   3.1 XRF 10
   3.2 SXRF 11
   3.3 SEM 11
   3.4 Model Samples 12
   3.5 MicroCT 13

4. Conclusions 14

Executive Summary

This innovative research drew on a suite of complementary materials characterization techniques to improve our understanding of tidelines on historical documents, books and artworks on paper. Tidelines, produced by wetting, interfere with the appreciation of historical artifacts and weaken the paper, predisposing it to further damage. This collaboration of Dartmouth College, the Library of Congress, and The Metropolitan Museum of Art has been the first part of an effort to further our understanding of tideline formation.

We used complementary non-invasive techniques to examine tidelines on historical samples and model samples produced to constrain confounding variables. We recorded the migration and deposition of inorganic materials associated with tidelines and investigated the effect of artificial aging on tidelines in sized and unsized model papers. This work produced new information about the inorganic chemistry associated with tidelines as well as visually arresting images of the chemistry and microstructure of tideline regions. The insights we gained will be useful to the scientific community and conservators, but raise further questions that we hope to answer with future work.

1. INTRODUCTION

Tidelines are residual damage on paper at a former wet/dry boundary, and are produced by environmental wetting or cleaning treatments (Bone et al. 1950; Dupont 1996; Koestler 2002). Although their typical brown coloration has led some to assume they are the result of the migration of soluble material from the paper or the wetting agent, tidelines can be created with pure water on purified cellulose (Eusman 1995). Even when tidelines are invisible to the naked eye, they can be seen in UV light, something which has been attributed to the presence of organic compounds produced by wetting (Eusman 1995). Previous work has shown that repeated wettings with increasing amounts of fluid will produce successive tidelines; and although previous lines may be overridden, they can still be observed under UV light. Thus tidelines represent irreversible (0.1 nm – 100 μm scale) changes to the chemistry and microstructure of the cellulose (Jeong et al. 2012).

Cotton cellulose is a long chain polymer. A hierarchical structure, elementary fibrils (1.5-3.5 nm) form microfibrils (10-30 nm) and microfibrilar bands (~100 nm), which are connected in a three-dimensional network to form a cell wall (diameter 15-100 μm). Paper has randomly oriented cellulose fibers, fibrils, and fines, and its microstructure is complex, multiscale, anisotropic, porous, and fundamental to its optical and transport properties (Ramaswamy 2001; Aaltosalmi 2004; Chinga-Carrasco 2008).

Cellulose is hygroscopic, and wetting produces three-dimensional microstructural changes in the fiber network. Individual fibers become less dense, straighter, and rougher, and there is an overall decrease in fiber-to-fiber contact, producing a more porous and weaker structure (Holmstad 2003). When wetted, cellulose fibers and structures swell and may undergo out of plane warping. The degree and direction of bulk deformation depends on fiber orientation (Ramaswamy 2001).

Structurally, drying is also transformative. Fibers shrink in width and lumens collapse, changing their shape, density and fiber-to-fiber contact area. This affects permeability and strength and produces the characteristic longitudinal wrinkles in previously wetted paper (Nanko and Ohsawa 1990). Other changes to fibers (e.g. straightening) or to their surface (e.g. roughening) during the wet/dry cycle could also irreversibly change the local microstructure.

Evidence of cellulose degradation and other chemical changes arising from hydrolysis and oxidation have been reported at the wet/dry interface (Zervos 2010). More specifically, degradation reactions have been related to the presence of hydroperoxides, which oxidize the pendent hydroxyls of cellulose to form aldehydes and conjugated ketones (these generating the characteristic brown color) (Łojewska et al. 2010; dupont). In addition, NOx and SOx absorb onto cellulose and desorb into water, creating acids that may also promote hydrolysis of cellulose (Zervos 2010).

This collaboration of Dartmouth College, the Library of Congress (LC), and The Metropolitan Museum of Art (MMA) is the first part of an effort to investigate and employ non-invasive techniques to study tidelines, in order to better inform treatment methodologie. Our objectives were: to further the scientific understanding of tideline formation in historical papers and model papers, to record the migration and deposition of inorganic material associated with tidelines through complementary *in situ* techniques,

and to further investigate the effect of artificial aging on tidelines in sized and unsized model papers. Our results included visually arresting images that visualize changes in tideline regions and improve our understanding of complexities faced by conservators when treating historical material on paper.

Our objective to produce micro computed tomography reconstructions (models) of fiber-pore microstructure in cellulosic substrates with which structural changes to the cellulose fiber in the tideline could be measured remains incomplete. The results to date are promising nonetheless, and will complement those reported here.

2. MATERIALS AND METHODS

We characterized changes across the wet-dry boundary of historical samples and model papers using scanning electron microscopy (SEM), scanning and mapping micro X-ray fluorescence (XRF), synchrotron XRF, and high resolution X-ray microcomputed tomography (microCT). We designed the study to include historical material as well as model samples that mimic historical materials. Some previous studies of model samples have only used Whatman number 1 filter paper, which is pure α cellulose. We have included Whatman No. 1 paper in order to relate our results to previous studies.

2.1 Sample Selection

Historical papers from the 18th and 19th centuries were selected from the Barrow Book Collection. William J. Barrow (1904-1967) conducted a series of scientific studies on the degradation of paper in 1963-1965 at the Virginia Historical Society. The Barrow Book Collection, which contains about 1000 books from 1507 to 1899, is housed in Preservation Research and Testing Division (PRTD) at the Library of Congress's Center for the Library's Analytical Science Samples (CLASS). The Barrow Books have the advantage of containing paper that has already been characterized in terms of provenance, paper type, and sizing, both by Barrow and later researchers through the present day.

We selected four Barrow Book collection samples with existing tidelines printed between the 17th and mid 19th century, shown in Table 1. All are gelatin sized as verified by chemical spot tests.

Table 1. Barrow Book Collection papers sampled

Number	Title	Place of Printing	Year	Paper Type
BB649	The Federalist on the New Constitution v1	New York	1802	Wove, pH 4.3, no carbonates, yes Al
BB717	The Oration of Demosthenes on the Crown	Boston	1868	100% cotton rag pH 5.0, no carbonates, yes Al
BB1077	The Modern Practice	London	1768	pH 4.5, no

	of Physic			carbonates, yes Al
BB1348	M. Tullii Ciceronis Opera Omnia	Amsterdam, Netherlands	1661	Laid, pH 5.7, no carbonates, yes Al

A page from Barrow Book #1077, The Modern Practice of Physic, is shown in both white and UV light in Figure 1. Although paper rattle and poor absorbency of pages without tidelines suggests fairly substantial sizing, there is a thick tideline on this page.

We also selected three non-accessioned works on paper, in the MMA's study collection. One was a botanical print from *Phytanthoza iconographia*, vol. 3: Ill. 607 (J. W. Weinmann, 1742), which we will call "Flowers." We tested two tideline regions on this sample (Figure 2).

Pre-modern papers typically contain impurities, due to processing conditions and the water used. Typical metal content in some pre-modern papers has been determined by XRF or ICP-MS and is (ppm): Ca, >10,000; Fe 200-300; K,200-1500; S, >500; Al, 100-1500; Mg, 100-800; S, 300-3000; Ca, 1000-6,000; K, 100-2000; Fe, 100-1000; Cu, <100 (. Even in modern manufacture, paper contains trace metals, as shown in information on ash content for Whatman No. 1 filter paper shown in Table 3.

Because we wanted to constrain some of the variables inherent to historical samples, we created tidelines under controlled conditions on some modern papers. Modern papers to be studied came from CLASS and the Conservation Division, the latter of which provided various samples of handmade paper made by the University of Iowa Center for the Book (UICB). CLASS holds a collection of well-characterized papers custom-made under the Institute for Standards Research (ISR) that are used as reference samples in libraries, archives and museums. Together these papers represent a range of materials found in cultural heritage collections, and the samples selected were strategically chosen to differ in additives such as gelatin, buffers, and starch sizing. In all, eleven types of paper were used to make the model samples. Many were ruled out after our preliminary examination revealed impurities that were judged uncharacteristic of historical samples. The papers are listed below:

- Whatman 1
- UICB Ptolemy
- UICB 2000
- UICB 1997
- UICB 2012
- Whatman 42
- Lana 2
- Lana 3
- Arches-Ingres
- Washed Khadi
- Stonehenge

Whatman 1, which became our standard, contains trace elements are shown in Table 2.

Table 2. Typical values (ppm) trace elements in Whatman 1

Calcium	185	Bromine	1
Sodium	160	Boron	1

Chlorine	130	Barium	<1
Nitrogen	23	Lead	0.3
Silicon	20	Chromium	0.3
Sulfur	15	Fluorine	0.1
Magnesium	7	Aluminum	<0.5
Iron	5	Manganese	0.06
Potassium	3	Antimony	<0.02
Zinc	2.4	Arsenic	<0.02
Copper	1.2	Mercury	<0.0005

Polarized light microscopy (PLM) was used to characterize the paper fibers used in the present study. The PLM analysis was done by Marina Ruiz Molina, Associate Conservator in the Paper Conservation Department at the MMA.

Tidelines were formed by vertical dipping of papers in about 2 cm of Millipore MilliQ deionized water for 15 hours in a room controlled at 25 °C and 50% RH , following methods used by previous researchers (Bone 1950; Eusman 1995; Dupont et al. 1996). lass or polypropylene trays used in this method were thoroughly pre-cleaned with alternating rinses of dilute nitric acid, ethanol and MilliQ water, followed by drying in an 80 °C oven to ensure that no trace elements were introduced from extraneous sources.

Model samples were then artificially aged for between 0 and 21 days in an 80°C oven at 65% RH. Additional Whatman No. 1 and UICB 2000 sized paper samples were pre-aged for 21 days before tideline formation as above. Strips were cut from large samples at select intervals for analysis, which was performed at LC, MMA and Dartmouth. Samples were stored in Mylar polyester enclosures and handled with gloves to protect them from oils or other contaminants.

2.2 X-ray fluorescence (XRF)

Two X-ray fluorescence (XRF) instruments were used to identify and map the distribution of elements below, above, and at the tidelines, to gain information about their displacement in the paper.

For XRF mapping, the MMA's Bruker M6 XRF system was used. This instrument has a 30W Rh-target microfocus X-ray tube, which was operated at 50 kV and 600 µA, a silicon drift detector, and polycapillary optics. The spot size used was 100 microns and the measuring head moved across the object surface in 100 micron steps, acquiring a full XRF spectrum at each point at 90 msec/pixel.

The Library of Congress' Bruker Artax XRF system has similar components, spot size, and resolution (Goel et al. 2006). The instrument was operated with He flushing at 40 kV and 700 µA to produce line scans as well as individual spot analysis, with either 90 second or 180 second exposure per spot.. The line scan spectra shown in the figures herein are autoscaled, or normalized.

XRF does not reveal light elements such as C, H, N or O. However, other elements associated with tidelines can be identified, including Al, Cl, and S, depending on their abundance; other elements normally found in paper, such as K, Ca, Mn, Fe, Cu and Pb, are easily detected by this technique.

2.3 Synchrotron XRF (SXRF)

Synchrotron sources produce the highest resolution for a variety of techniques including 30-40 nm resolution XRF (Chinga-Carrasco 2008; Samuelsen et al. 2001; Antoine et al., 2002, Holmstad et al. 2005, 2006; Goel et al. 2006; Vernhas et al. 2008). We used the hard X-ray nanoprobe at APS beamline 26-ID (resolution: 60 nm). While the field of view for maximum resolution is 15 μm, samples up to 1 cm^2 can be accommodated.

We proposed and received 36 shifts (288 hours) of beam time for XRF and nanotomography at the Argonne National Laboratory's Advanced Photon Source (APS). We used nine shifts of this in March (2017-1) at 32-ID. Sector 32 had recently divested itself of its nanotomography capabilities (these now reside at Sector 2), so in March we were able to do XRF only. We applied for additional beam access in 2017-2 (summer 2017) but didn't receive it. We therefore have not yet been able to do truly nanoscale tomography, and have 27 shifts of unused beam time at APS (valid until March 2018).

At Dartmouth, Obbard and student Jing Ting (Lily) Zhang designed a universal sample holder that could be used to transfer samples between Cornell and Argonne without remounting them (thus enabling a specific area to characterized with both techniques). These were designed in SolidWorks and 3D printed at Dartmouth (Figure 3).

Obbard, Zhang, and two other undergraduate students visited the Advanced Photon Source at Argonne National Laboratory in March 2017. A problem with the APS stage prevented our most efficient usage of this beam time. Also, as with any first synchrotron visit in a series, considerable time was spent establishing the optimal scanning conditions, focusing the beam on a sample, finding an area of interest, and interpreting results. Two papers were scanned during the visit, Whatman No. 1, and Barrow Books Collection 1348. A second beam time request was submitted to take advantage of our significant remaining beam time this summer, but was turned down due to the shear number of competing requests.

2.4 Scanning electron microscopy-energy dispersive X-ray spectroscopy (SEM-EDS)

Scanning electron microscopy (SEM) and energy dispersive spectroscopy (EDS) are being used to analyze the surface structure and chemical composition at, above, and below tidelines. We examined model papers without and with tidelines and historical papers with old tidelines. At Dartmouth, we used an FEI XL-30 in environmental mode (uncoated samples) at 15 keV and an EDAX Energy Dispersive Spectroscopy system (EDS). In order to find the tidelines on the samples once in the SEM, we marked each tideline with three or four small holes made with the tip of a tungsten needle. We captured images of the tideline at 200X and collected EDS spectra from three 100 x 100 micron areas above, on and below the tideline. At LC and FEI Quant was used.

2.5 X-ray micro computed tomography (microCT)

X-ray micro computed tomography (microCT) can provide nondestructive three dimensional (3D) internal structural characterization of small, porous or multiphase

samples. A sample is held between an X-ray source and detector and rotated 180° or 360° in discrete steps with an X-ray attenuation image taken at each step. The image is projected onto a scintillator, which converts the X-rays to visible light images that are captured by a high resolution CCD camera. Contrast resolution in microCT images depends on the X-ray attenuation characteristics of the phases present, a function of mass density and composition, on X-ray energy, and on the range of intensities captured by the camera. The set of X-ray attenuation images is reconstructed to produce a stack of horizontal cross sections of the sample. A volume of interest (VOI) is chosen and the cross sections are binarized by applying thresholds to distinguish between ice, brine and air. The stacks of binary images are then reconstructed to produce a 3D image of the internal structure of the object. Post processing can produce visualizations of this structure, and over three dozen different quantitative metrics can be gathered from the reconstructed models, including the number, size, shape, volume and orientation of 'objects' of each phase (cellulose fibers in this case).

For this project, we used an Xradia 520 Versa microCT at the Cornell University School of Biotechnology. We sent 4x4 mm mounted samples to Cornell. We started with a 1hour scan at 6.94 micron resolution. We then tested 2.5 hour and 8 hour scans. The 8 hour scans provided the best resolution (~0.77 micron) but were costly, so we scanned only the samples we thought likely to be the most representative (and only unsized samples). Samples tested with MicroCT are shown in Table 3.

Table 3. Samples scanned in Xradia 520 Versa. Aging refers to artificially produced tidelines on model samples. Location is with respect to the tideline (A=above, TL=on tideline, B=below)

Sample	Aging (days)	Location	Scan resolution (microns)	Comment
Whatman 1	21	A, TL, B	0.84	
Whatman 1	0	TL	0.77	Run in triplicate
Whatman 1	21	TL	0.77	
Whatman 1 with pre-aging	0	TL	0.77	
Whatman 42	0	TL	0.77	
UICB Ptolemy	0	TL	0.77	
Barrow 1348	n/a	TL	0.75	

2.6 Tensile Testing

Tensile testing was done on "dogbone" tensile test specimens cut from a model sample prepared sheet of Whatman 1 (unaged) to compare the strength of the paper at the tideline to its strength in the regions above and below the tideline. The paper was cut using an ASTM standardized type V D638 steel die, creating dog-bone shaped samples 64 mm long and 9mm wide, with a narrow section of 1-dimensional stress 10 mm long and 3 mm wide. Twenty samples were cut such that the tideline ran across the narrow

section of the paper. Ten samples were cut 10 cm above the tideline and ten below the tideline. All had their long axis oriented in the machine direction (the Whatman 1 did have a preferential fiber orientation).

Each sample was tested until it tore, in an Instron 4442 Universal Testing System, at a strain rate of 3 mm/min and 500 N.

3. RESULTS AND DISCUSSION

In the model samples that had tidelines formed in the laboratory, these tidelines ran across the entire width of the paper sample and had an approximate width of 0.5 mm. Although the historical samples (e.g. BB#1077) containing tidelines were all sized, and also formed new tidelines, no modern gelatin sized papers produced visible tidelines This included the sized UICB 2000 paper, which was pre-aged prior to the tideline experiment. However, UV light examination (365 nm) showed a faint fluorescence at the water immersion line in these samples. This suggests that undegraded sizing effectively prevents vertical transport of water and thus provides protection against tideline formation. Results also suggest that sizing will naturally break down in conditions not represented by the artificial pre-aging, and allow tideline formation.

Artificial aging of tidelines generally produced darkening from yellow to brown. In addition, aging of the tideline formed on the Whatman No.1 paper produced gradual diffusion of some elements and showed a distinctive multi-zone appearance in UV light after 21 days (Figure 4). While not as obvious, there were suggestions of a similar phenomenon on the unsized UICB paper after 21 days of aging.

3.1 XRF

The botanical print from Phytanthoza iconographia, labeled as “Flowers”, was tested with the Bruker M6 at the MMA only. Major elements identified in association with the tideline in both regions tested were S, K, and Cl (Figures 5 and 6). S and K are concentrated at leading edge, while Cl is distributed more evenly across the wetted area. In the upper right hand region, copper was also associated with the tideline, and this is most likely due to the presence of pigment.

In other samples, the XRF line scans acquired with the Bruker Artax produced complementary information. Results from the existing tideline on a page from Barrow Book #1077 are presented in Figure 7. The XRF maps show how the elements of interest are distributed with respect to the visible tideline. S and K are concentrated at the tideline. Fe is present also in the tideline, but not as concentrated. Ca and Cl are insignificant. The line scan (spectra autoscaled, or normalized) includes these elements as well as Al, P, Mn, Fe, Cu, Zn and Pb. Here, all of the elements show a pattern of increased concentration just below and in the visible tideline. There is even a hint of a double tideline.

A new tideline was produced on this same paper using MilliQ water as described above. The XRF elemental maps (Figure 8) show that S, K and Cl swept from the wetted area to the tideline; Fe and Ca are also slightly concentrated at the tideline. This tideline is much sharper and more pronounced than the historical one (age unknown), and the area under the tideline appears much lighter in color, i.e. cleaner. There are several

possible reasons for this: 1) the sizing has likely degraded over time, permitting better transport of both impurities and accumulated degradation products, 2) the cellulose has undergone changes during aging that improve transport of the same materials, 3) the original tideline was sharper and has diffused over time, and 4) the area under the tideline has changed over time.

The linescan presented in Figure 8 shows some additional information. Note the offset of the elements with respect to the vertical position of the visible tideline. The paper is essentially behaving as a thin layer chromatography (TLC) substrate. Mn and Zn appear at the front of the tideline, Ca and S at the back, and K in the middle. Mn and Zn likely originate in the paper. Overall we see a strong concentration of what had been minor elements in the paper, including transition metals, swept to the tideline. Although these results are qualitative, they show very good signal to noise ratio, because the concentrations of these elements are now significant. We plan to run some standards to quantify them before publication.

All of the unsized model papers formed tidelines with strong concentrations of S, K, and Cl (Figure 9). Gelatin-sized model papers did not form tidelines visible with the naked eye, although UV revealed some fluorescence at the water line in all of these samples. The second through fifth samples in this set are Whatman 1 paper. In these samples, the tidelines appear to have become more diffuse with aging, particularly regarding the concentrations of K and Cl. In the manufacturing process, the unsized UICB Ptolemy papers are treated with Ca (liming, not buffering) and therefore Ca is visible at the tideline.

3.2 SXRF

Synchrotron XRF element maps for Whatman 1 are shown in Figure 10. Note that the elements are shown in order of their atomic number. The energy of the emitted photon is characteristic of the element from which it fluoresced. Lower atomic number elements have lower energy characteristic X-rays, so detection limits vary by element and, in this case we could not detect sodium. While there is no optical image of the area scanned, the maps reveal the fiber structure as some elements, e.g. sulfur and chlorine, are very clearly associated with fibers, while others are not. The Ca, for instance, is primarily seen in a particle that also contains Al and Si. This could be a mineral particle.

While the techniques used here identify only elements, and not chemical groups or compounds, the colocation or lack thereof of certain elements are clues. For instance, we may wonder what form of S, K, and Cl are co-located with the fibers at the tidelines. These maps suggest that it is probably not $CaSO_4$ or CaCl, but do not rule out KSO_4 or KCl.

It is also quite interesting to see metals, including Si, Cu, and Mn, in the maps, not only as particulates, but associated with the fibers themselves. This suggests that there is more chemistry going on than we understand. Could the Cu be present as copper sulfate?

3.3 SEM

Although we marked the tideline with a series of small holes so we could identify it in the SEM, we found that it was possible to do so in many cases by the brightness of the backscattered electron (BSE) image of the surface at the tideline. One could detect the tideline on BSE images of Whatman 1 (Figure 11) and UICB Ptolemy (Figure 12) samples by the presence of many fine bright particles or overall brightness in that region. With EDS, these were found to contain S, Na, Ca, and Cl. In contrast to the unaged tideline made on Whatman 1 (Figure 10), the sample aged for 21 days still showed a bright region around the tideline (holes) but the heights of the S, Na, Ca, and Cl peaks was greatly reduced relative to the C and O peaks. This is interesting when compared to the UV and XRF results, which both suggest diffusion from TL with aging (Figures 5 and 10).

Similar results were obtained from the SEM/EDS at LC. Here, we were able to produce false color maps, which highlight the particles and allow us to see which elements are co-located (Figure 13). We found that S strongly associated with both Na and Ca in particulate matter.

False color element maps of the unsized UICB (Ptolemy) paper after 21 days of aging (Figure 14) shows the development of overlapping zones of element concentration, S, Ca, and Mg. No K or Cl were detected.

SEM/EDS elemental mapping of the laboratory-made tideline on a sample from Barrow Book 1077 revealed collocated particles containing Ca and S (Figure 15). This could be $CaSO_4$, but we can't know for sure.

3.4 Model Samples

It was observed that aging after tideline formation causes further movement of the elements, particularly chlorine and potassium, accumulated at the wet-dry interface when the tideline was initially formed. It appears that the University of Iowa Center of the Book Ptolemy paper samples mimicked the historical Barrow book samples in content and distribution around the tidelines.

Interestingly, we have found that the visible and UV photos of the gelatin sized papers, there were almost no fluorescence was formed at the wet-dry interface, and no tidelines formed above the wet-dry interface. This was remarkable because most historical samples of tidelines were formed on gelatin-sized paper. However, since the sample UICB 2000 sample immersed for 53 hours and 23 minutes began showing fluorescence at day 20 of aging, this suggests that tidelines, thus alteration, form slowly and are sometimes not detectable until later. The role that gelatin sizing in resisting the tideline formation, the process of its degradation, and how that may affect the tideline are future topics to be investigated.

Figure 3 shows the elemental maps from the upper right hand tideline area, shown with a photograph of that region for reference (upper left). Note how the S and K (sulfur and potassium) are most concentrated in the edges of the tideline, while the chlorine is more diffuse.

Figure 4 shows the elemental maps from the bottom right hand tideline area. Here again the tideline seems to have swept up and concentrated the chlorine, sulfur and potassium, although the concentration of the sulfur at the edges is more pronounced.

3.5 MicroCT

Figure 16 is an image produced by Cornell (Teresa Porri) using Osirix, a medical imaging viewer. Osirix is useful for visualization, but doesn't produce images that can be queried for quantitative data. Figure 17 shows an orthogonal projection of a microCT reconstruction made with the XRadia software native to the collection instrument. It could be used for quantitative analysis, but because we don't have the Xradia software at Dartmouth, and would have needed to incur travel expenses to travel to Cornell to use it, we have worked on producing reconstructions using other software.

An undergraduate student (Mackenzie Kynoch) made promising progress on this front in Spring 2017, so in Summer 2017, we requested and received a small grant from Dartmouth's Neukom Institute for her to continue this work (the Neukom Institute funds scientific research in which computational methods are integral to progress). One of the difficulties was that the stacks of reconstructed images produced by the XRadia instrument were in DICOM (Digital Imaging and Communications in Medicine) format. We had planned to produce models using the software associated with our (Dartmouth) Bruker Skyscan microCT, but found that it doesn't read DICOM format files. A colleague at Dartmouth had used an FEI microCT system, and allowed us to use FEI Amira software, which can use imported DICOM stacks. Mackenzie produced the images shown in Figure 18 with Amira.

We found that the open source NIH Image J software (FIJI) can create a 3D visualizations (Figure 19), but like Osirix, it cannot produce a volume that can be exported and analyzed.

The ability to derive quantitative data from 3D models is key to our analysis of structural changes to the fiber at the tideline. Simple segmentation of fiber from air in the 3D models will allow us to measure bulk porosity, but it is well known that porosity is highly dependent on local humidity. If we can isolate individual fibers within the 3D models, we can produce statistical data on the fiber level. Metrics such as: fiber volume, fiber surface area, surface to volume ratio, fiber thickness, surface convexity, and anisotropy (or length to width ratio) are possible and would help us understand what structural changes are associated with tidelines. Are fibers shorter? (that would decrease strength) Are they rougher? (that might mean fraying, or breakage of microfibrils) Does the decrease in fiber to fiber contact that takes place with wetting (Holmstad et al., 2003) remain? And can we discriminate between this effect and the collapse of lumen during drying (Nanko and Osawa, 1990)? Separately or together they could decrease strength.

In order to know the answers to these questions, we need to discriminate one fiber from another in the cellulose phase model produced by microCT. This is known as a segmentation problem. There is a computational method for problems such as this. The "watershed transform" is a method of image processing developed by geomorphologists. It segments an image so that objects of interest are separated from the background and, importantly, from neighboring objects of the same type. The basic concept behind this method is that local minima and the lines at which those minima meet is analogous to a topographic surface being flooded. The "catchment basins" are filled with "water" first, and at the lines where those basins meet watershed lines are formed (Roerdink et al.

2001). The algorithm will identify basins by finding points that are closer to a local minimum point than to any other minima in the region. The watershed will be those points that do not belong to any catchment basin. There exist several methods for implementing the watershed transform, including a continuous case, discrete case, an algorithmic calculation through simulated immersion, and a calculation by topographical distance. The main difference between these methods is whether the watershed is determined through simulation or direct calculation.

There exists a Matlab toolbox for implementing the watershed transform (Eddins 2002). Now funded by a Junior Undergraduate Research Grant from Dartmouth's Undergraduate Advising and Research Department, Mackenzie is using Matlab to produce 3D models of the Whatman 1 image stacks (first converting them from DICOM to bitmap) and planning to use the watershed transform to segment them.

4. Conclusions

Our analysis of laboratory-produced tidelines on historical material and on model samples that mimic historical materials has helped bridge the gap between tidelines created in pure cellulose and those observed in historical papers. It also suggests some new or at least more informed questions about the nature of tidelines and specifically tideline products. Our conclusions and the questions they raise follow:

Modern gelatin sized samples immersed for 15 hours did not form tidelines visible to the naked eye. While UV showed a faint fluorescence at the water line in these samples, it located at the level of the water bath and did not indicate migration. A UICB 2000 (sized) sample immersed for 53 hours and 23 minutes began showing fluorescence at day 20 of aging, suggesting that longer immersion or aging permits tidelines to form.

Thus sizing prevents vertical transport of water and provides protection against tideline formation, but not indefinitely. Tidelines formed readily in historical papers with gelatin sizing, implying that the sizing breaks down with time.

We found that S, K and Cl are typically concentrated at the leading edge of a tideline produced on modern unsized paper and that these elements are associated with the fibers themselves. We don't know what form these elements take. Salts of sodium and potassium (i.e. KSO_4 and KCl) are soluble in water, as are many other sulfates.

In historical tidelines and in tidelines on modern unsized papers after 21 days of aging, the Cl was no longer strongly present at the tideline (e.g. in Flowers, In BB #1077, and in Whatman 1 and UICB Ptolemy after aging). *Is the Cl leaving the paper and if so, how?*

In both historical and modern model samples, linescan XRF and SXRF reveal a surprising accumulation of elements at the tidelines, including a number of transition metals, which are well known to catalyze autooxidation of cellulose. Other metals detected by XRF include Si, Ca, and K, along with non-metals S and Cl. SEM/EDS analysis showed that Na and Mg are also prevalent at some tidelines, and that Na, Mg, Ca and K are often co-located with S in particulate matter. While the presence of carbonates cannot be discounted, sulfate salts formed at tidelines are not expected to act as buffers, as has been hypothesized (Jeong). Furthermore, synchatron XRF and SEM/EDS suggested that not all metals carried to the tideline form salts, rather Si, P, Cu, and Mn

appear to be associated with the fibers themselves. Therefore, it is not known at present what role the elements detected at tidelines play in resulting cellulose properties and stability.

Under future funding, we plan to investigate to which compounds are present at tidelines and determine whether they were moved there or formed *in situ*. We also hope to determine the best method of implementation of the watershed transform to microCT images of paper in order to segment the sample for microstructural analysis on the fiber level. This will constitute a novel application of the watershed transform and a breakthrough for the cellulose science and conservation communities.

PRODUCTS

Project Website

TOPS Talk
Topics in Preservation Lecture - The Library of Congress offers free public programs to share basic preservation information and practical advice and to raise awareness of preservation issues for our cultural heritage. 'Topics in Preservation' Series lectures are held at the LC, and streamed live by webcam. Those who are unable to attend in person or stream the live feed can access the lecture within a few months via high-quality on-demand stream.

Paper Samples – Currently held by the LOC, MMA, and Dartmouth.

ENGS 24 Group Final Report – documents progress in SEM image segmentation, tensile testing, and tomographic analysis.

Cornell Xradia reconstructed microCT files . Currently help on ThayerFS File Server at Dartmouth College. Can make available when we are done our microCT analysis.

ACKNOWLEDGEMENTS

R. Obbard and L. Zhang were funded by the National Center for Preservation Technology and Training, Preservation Technology and Training Grants Program (Award P16AP00359), National Parks Service, Department of the Interior.

L. Brostoff and S. Centenno were funded by the Library of Congress and The Metropolitan Museum of Art, respectively. Mackenzie Kynoch was funded by the Neukom Institute at Dartmouth College.

This research used resources of the Advanced Photon Source, a U.S. Department of Energy (DOE) Office of Science User Facility operated for the DOE Office of Science by Argonne National Laboratory under Contract No. DE-AC02-06CH11357.

We also thank Marina Ruiz Molina, Paper Conservator, Paper Conservation Department, MMA; Tana Villafana, Andrew Davis, Eric Monroe, and Fenella France, Library of Congress; and Z. Cai, I. McNulty, and V. Rose, Argonne APS Beamline 26-ID-C scientists.

REFERENCES

Aaltosalmi, U., M. Kataja, A. Koponen, J. Timonen, A. Goel, G. Lee and S. Ramaswamy. 2004. "Numerical analysis of fluid flow through fibrous porous materials", *Journal of Pulp and Paper Science*, 30 (9): 251.

Antoine, C., P. Nygård, Ø.W. Gregersen, T. Weitkamp and C. Rau. 2002. "3D images of paper obtained by phase-contrast X-ray microtomography: image quality and binarisation", *Nucl. Instrum. Meth. A*., 490 (1-2): 392-402.

Bone, W.A. and H.A. Turner. 1950. "Some effects of the evaporation of water from cotton cellulose", *Journal of the Society of Dyers and Colourists*, 6(6):315.

Chinga-Carrasco, G., M. Axelsson, Ø. Eriksen and S. Svensson. 2008. "Structural Characteristics of Pore Networks Affecting Print-Through", *Journal of Pulp and Paper Science*, 34 (1): 13-22.

Dupont, A.L. 1996. "Degradation of cellulose at the wet/dry interface. 1.The effect of some conservation treatments on brown lines", Restaurator-*International Journal for the preservation of Library and Archival Material*, 17(1):1-21 doi: 10.1515/rest.1996.17.1.1

Eddins, Steve (2002) The Watershed Transform: Strategies for Image Segmentation. Mathworks. Retrieved from: https://www.mathworks.com/company/newsletters/articles/the-watershed-transform-strategies-for-image-segmentation.html

Eusman, E. 1995. "Tideline formation in paper objects, cellulose degradation at the wet-dry boundary" in: Studies in the History of Art; 51: 10-27.

Holmstad, R., C. Antoine, P. Nygard and T. Helle. 2003. "Quantification of the three-dimensional paper structure: methods and potential", *Pulp and Paper Canada*, 104 (7):47-50. http://www.chemeng.ntnu.no/research/paper/Publications/2002/Manuscript_R_Holmstad_A4_2.pdf

Goel, A., C.H. Arns, R. Holmstad, O.W. Gregersen, F. Bauget, H. Averdunk, R.M. Sok, A.P. Sheppard and M.A. Knackstedt. 2006. "Analysis of the impact of papermaking variables on the structure and transport properties of paper samples by x-ray microtomography", *Journal of Pulp and Paper Science*, 32:111-122.

Holmstad, R., Ø.W. Gregersen, U. Aaltosalmi, M. Kataja, A. Koponen, A. Goel and S. Ramaswamy. 2005. "Comparison of 3D structural characteristics of high and low resolution X-ray microtomorgraphic images of paper", *Nord. Pulp Pap. Res. Journal*, 20:283-288.

Holmstad, R., A. Goel, S. Ramaswamy and Ø.W. Gregersen. 2006. "Visualization and characterization of high-resolution 3D images of paper samples" *Appita Journal*, 59: 370-377.

Jeong, M.-J., A.-L. Dupont and E.R. de la Rie. 2012. "Degradation of cellulose at the wet-dry interface: I - study of the depolymerization", *Cellulose*, 19: 1135-1147. http://link.springer.com/article/10.1007/s10570-012-9722-4/fulltext.html

Koestler, R.J., V.H. Koestler, A.E. Charola, F.E. Nieto-Fernandez (eds) "Art, Biology, and Conservation: Biodeterioration of Works of Art", Conference Proceedings, June 13-15, 2002; NYC; c. The Metropolitan Museum of Art, New York.

Łojewska, T.; Miśkowiec, P.; Missori, M.; Lubańska, A.; Proniewicz, L. M.; and J. Łojewska. 2010. "FTIR and UV/vis as methods for evaluation of oxidative degradation of model paper: DFT approach for carbonyl vibrations", *Carbohydrate Polymers*, 82: 370–375.

Nanko, H. and J. Ohsawa. 1990. "Scanning laser microscopy of the drying process of wet webs", *Journal of Pulp and Paper Science*, 16: 6-12.

Ramaswamy, S., S. Huang, A. Goel, A. Cooper, D. Choi, A. Bandyopadhyay and B.V. Ramaro. 2001. "The 3D structure of paper and its relationship to moisture transport in liquid vapor forms", The science of papermaking – 12th Fundamental research symposium, Oxford, UK, 2-3: 1289 & 1641.

Roerdink, Jos B.T.M, Meijster, Arnold. (2001). The Watershed Transform: Definitions, Algorithms and Parallelization Strategies. Fundamenta Infomaticae. Vol 41:187-228.

Samuelsen, E.J., T. Helle, P-J. Houen, Ø.W. Gregersen and C. Raven. 2001. "Three-dimensional imaging of paper by use of Synchrotron X-Ray Microtomography", J. Pulp Pap. Sci., 27 (2): 50-53. http://www.chemeng.ntnu.no/research/paper/Publications/1999/samuelsen-papfy3D.pdf

Zervos, S. 2010. "Natural and accelerated ageing of cellulose and paper: A literature review", In Cellulose: Structure and properties, derivatives and industrial uses. Eds. Lejeune, A. and Deprez, T. New York, Nova Publishing.

NOT CITED – saving in case we need them

Ali, M., A.M. Emsley, H. Herman and R.J. Heywood. 2001. "Spectroscopic studies of the ageing of cellulosic paper". Polymer, 42 (7), 2893-2900. http://www.sciencedirect.com

Bicchieri, M., A. Sodo, G. Piantanida and C. Coluzza. 2006. "Analysis of degraded papers by non-destructive spectroscopic techniques", *Journal of Raman Spectroscopy*, 37 (10), 1186-1192.

Castro, K., E. Princi, N. Proietti, M. Manso, D. Capitani, S. Vicini, J.M. Madariaga and M.L. De Carvalho. 2011. "Assessment of the weathering effects on cellulose based materials through a multianalytical approach", *Nuclear Instruments and Methods in Physics Research Section B: Beam Interactions with Materials and Atoms*, 269 (12), 1401-1410. http://www.sciencedirect.com/science/article/pii/S0168583X11003302

Chinga-Carrasco, G. 2009. "Exploring the multi-scale structure of printing paper-a review of modern technology", Journal of Microscopy, 234 (3): 211-242. http://onlinelibrary.wiley.com/doi/10.1111/j.1365-2818.2009.03164.x/full

Kavkler, K. and A. Demšar. 2011. "Examination of cellulose textile fibres in historical objects by micro-Raman spectroscopy", *Spectrochimica Acta Part A: Molecular and Biomolecular Spectroscopy*, 78 (2), 740-746 http://www.sciencedirect.com/science/article/pii/S1386142510006165

Łojewska, J., P. Miśkowiec, T. Łojewski and L.M. Proniewicz. 2005. "Cellulose oxidative and hydrolytic degradation: In situ FTIR approach." *Polymer Degradation and Stability*, 88 (3), 512-520. http://www.chemia.uj.edu.pl/~malek/2005Miskowiec2.pdf

Niskanen, K. and H. Rajatora. 2002. "Statistical geometry of paper cross-sections", *Journal of Pulp and Paper Science*. 28: 228–233.

Vernhes, P., J.F. Bloch, C. Mercier, A. Blayo and B. Pineaux. 2008. "Statistical analysis of paper surface microstructure: A multi-scale approach", *Applied Surface Sci*., 254: 7431-7437. http://www.sciencedirect.com/science/article/pii/S0169433208013809

Wiltsche, M., M. Donoser, W. Bauer, H. Bischof. 2005. "Advances in Paper Science and Technology: Transactions of the 13th Fundamental Research Symposium", 103: 853-899

Figure 1. BB #1077, "The Modern Practice of Physic", Vol. 1, London, 1768. Tideline as seen in normal light (left) and UV light (right).

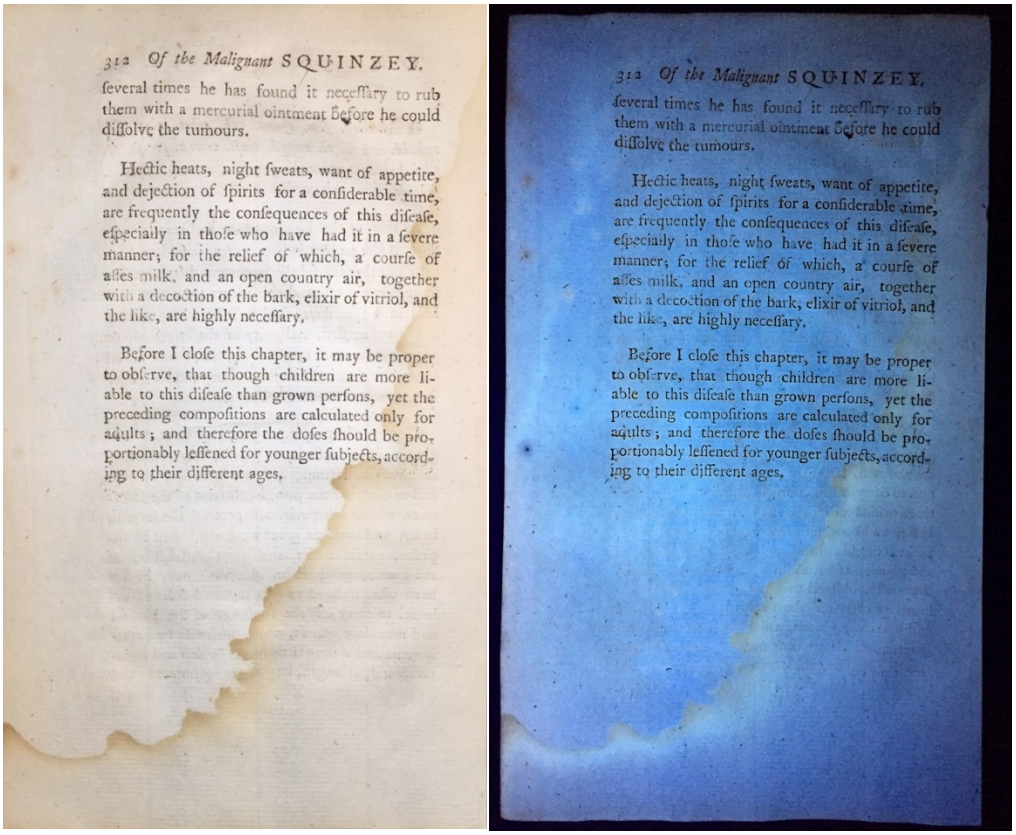

312 *Of the Malignant* SQUINZEY.

ſeveral times he has found it neceſſary to rub them with a mercurial ointment before he could diſſolve the tumours.

Hectic heats, night ſweats, want of appetite, and dejection of ſpirits for a conſiderable time, are frequently the conſequences of this diſeaſe, eſpecially in thoſe who have had it in a ſevere manner; for the relief of which, a courſe of aſſes milk, and an open country air, together with a decoction of the bark, elixir of vitriol, and the like, are highly neceſſary.

Before I cloſe this chapter, it may be proper to obſerve, that though children are more liable to this diſeaſe than grown perſons, yet the preceding compoſitions are calculated only for adults; and therefore the doſes ſhould be proportionably leſſened for younger ſubjects, according to their different ages.

312 *Of the Malignant* SQUINZEY.

ſeveral times he has found it neceſſary to rub them with a mercurial ointment before he could diſſolve the tumours.

Hectic heats, night ſweats, want of appetite, and dejection of ſpirits for a conſiderable time, are frequently the conſequences of this diſeaſe, eſpecially in thoſe who have had it in a ſevere manner; for the relief of which, a courſe of aſſes milk, and an open country air, together with a decoction of the bark, elixir of vitriol, and the like, are highly neceſſary.

Before I cloſe this chapter, it may be proper to obſerve, that though children are more liable to this diſeaſe than grown perſons, yet the preceding compoſitions are calculated only for adults; and therefore the doſes ſhould be proportionably leſſened for younger ſubjects, according to their different ages.

Figure 2. Botanical print from Phytanthoza iconographia, vol. 3: Ill. 607 (J. W. Weinmann, 1742), recto (top) and verso (bottom), referred to as “Flowers” in the text.

Figure 3. Custom designed sample holder, designed in SolidWorks (top) and 3D printed (bottom left). In beamline at APS (bottom right).

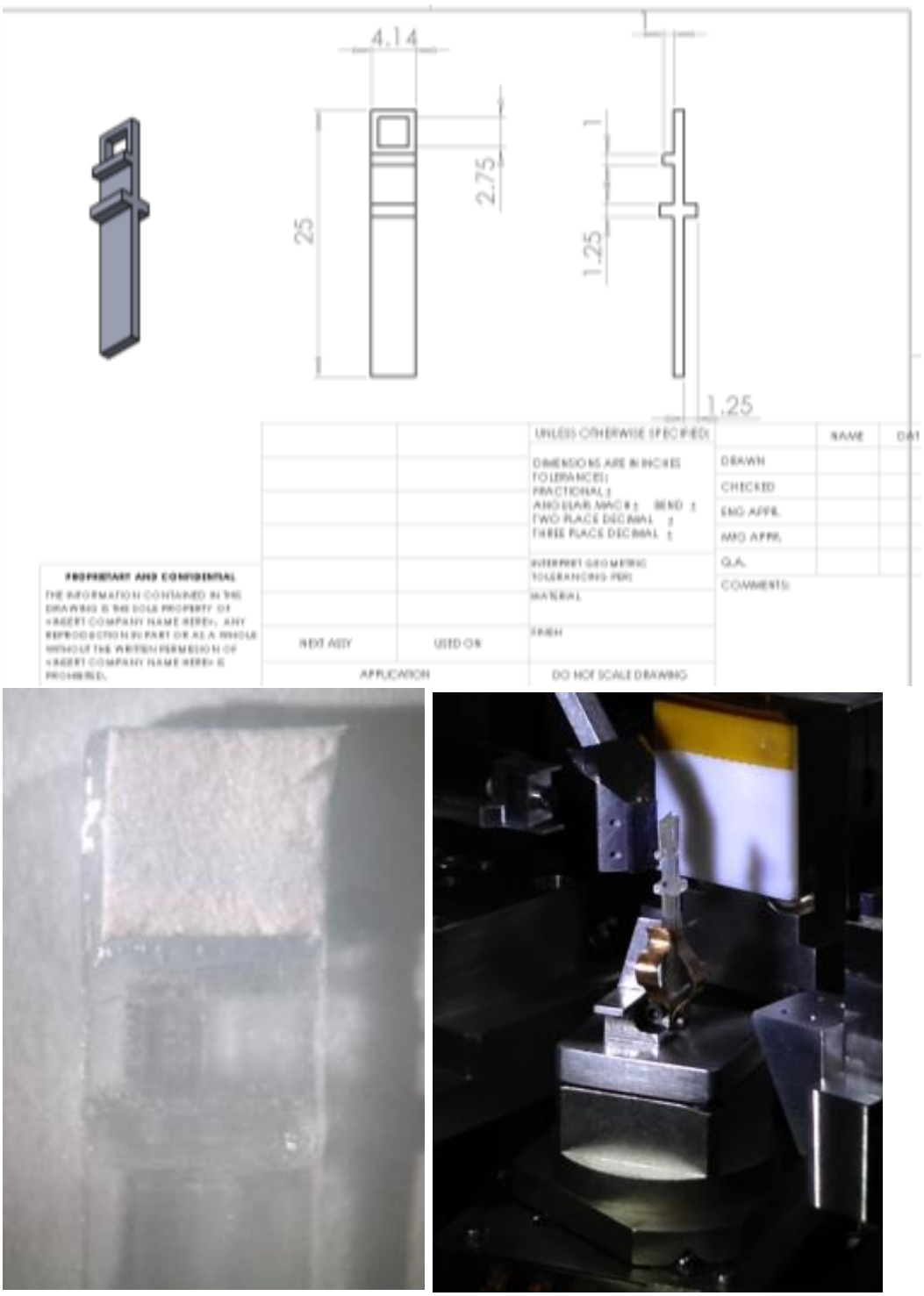

Figure 4. Laboratory produced tideline on Whatman 1 paper after 21 days of artificial aging as described in the text in white light (left) and UV (right).

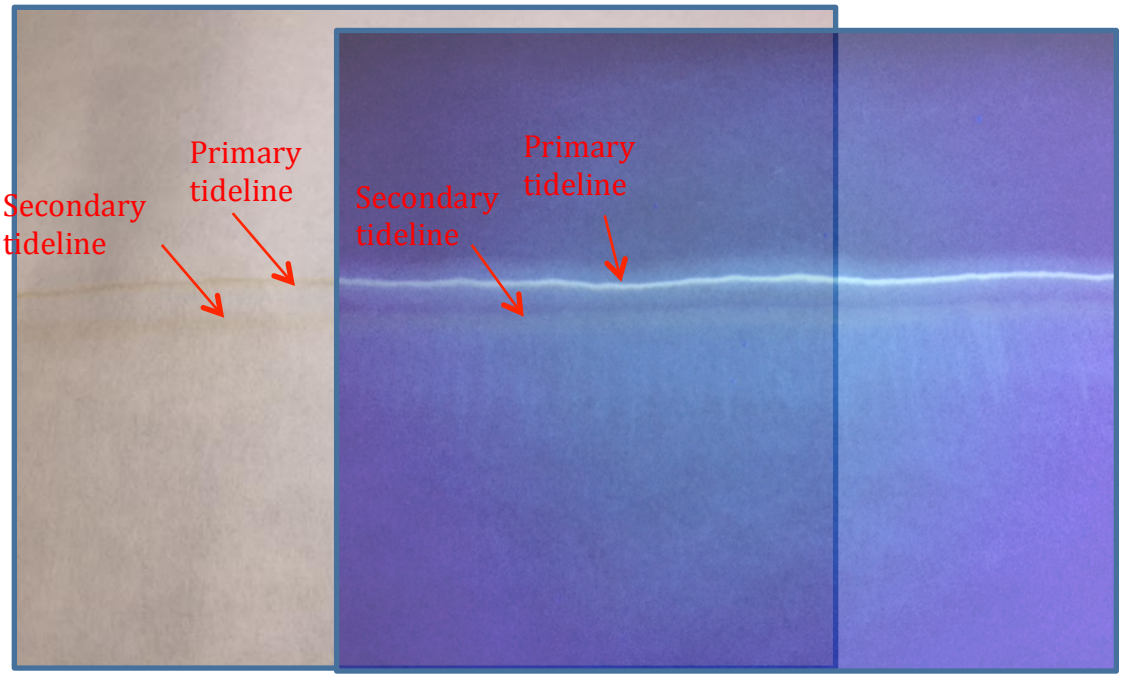

Figure 5. Elemental maps acquired in the upper right hand tideline area of “Flowers”, shown with a photograph of that region for reference (upper left). Note how the S and K (sulfur and potassium, pink and light blue maps) are most concentrated in the edges of the tideline, while the Cl is more diffuse.

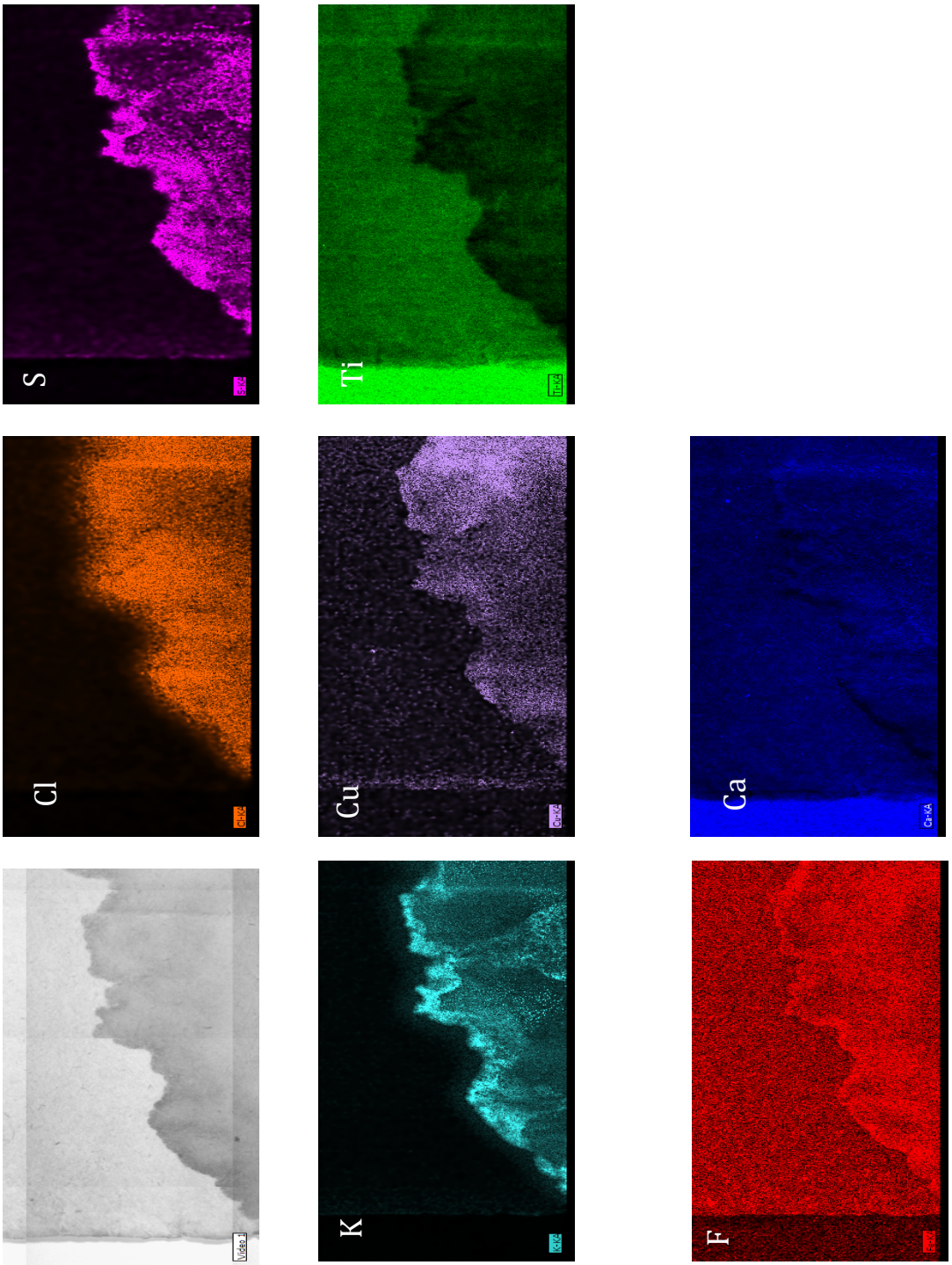

Figure 6. Elemental maps acquired at the bottom right hand tideline area of “Flowers”. Also in this area, the tideline seems to have swept up and concentrated the S, K, and Cl.

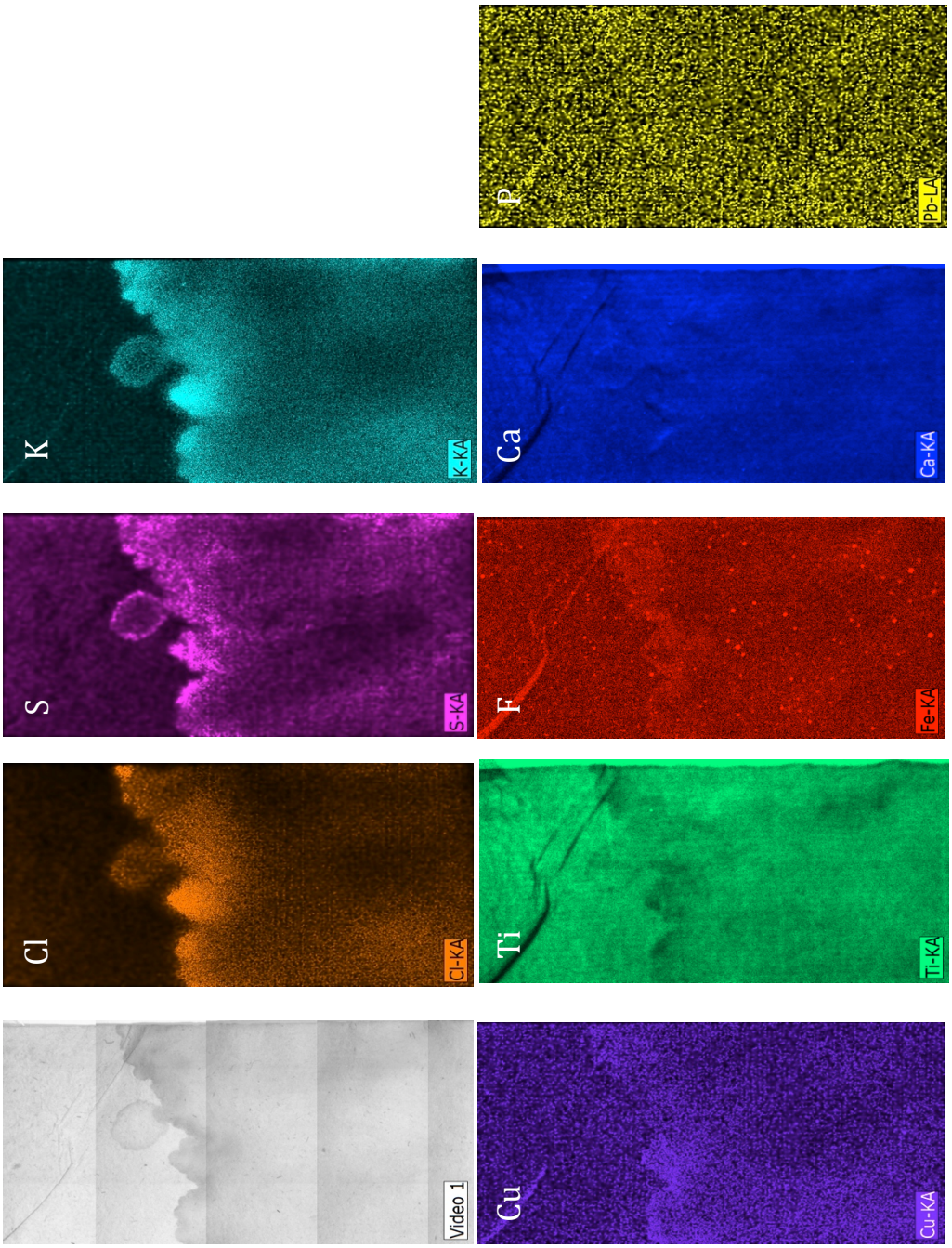

Figure 7. XRF maps (left) and line scans (right) acquired on an existing tideline on Barrow Book #1077 – “The Modern Practice of Physic” (1768).

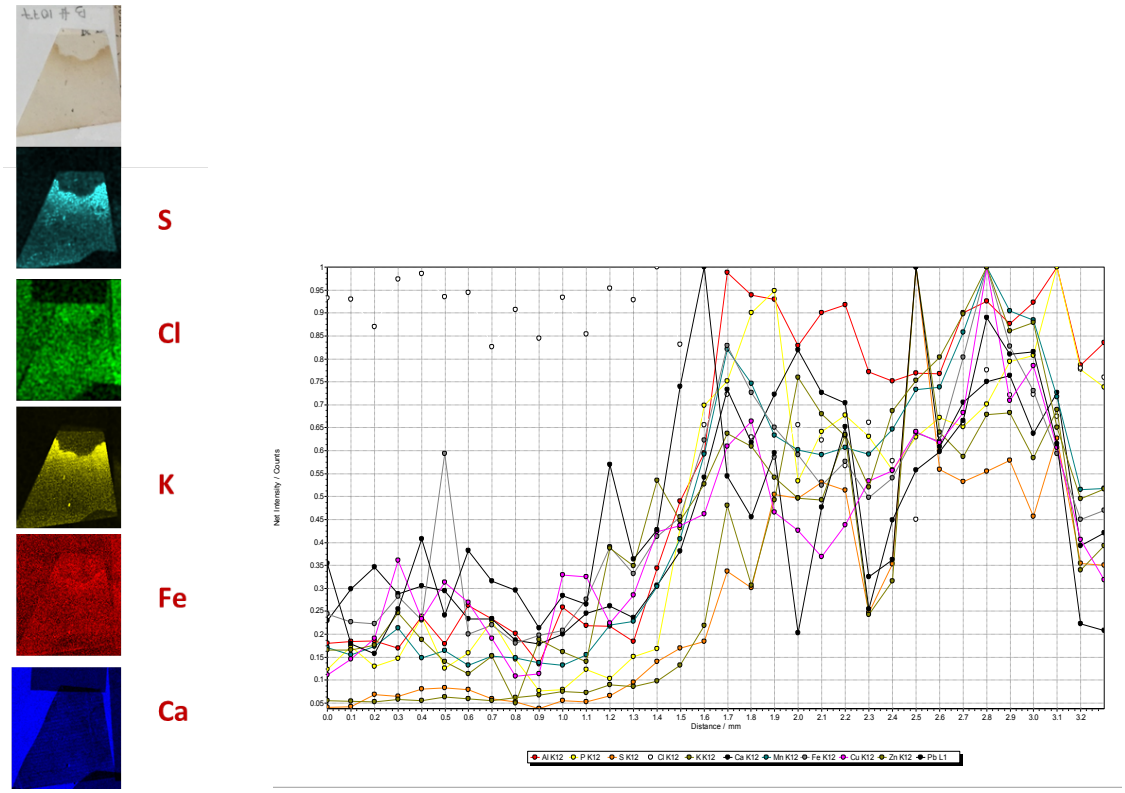

Figure 8. XRF maps (top) and line scans (bottom) acquired in a newly created TL on BB #1077 – “The Modern Practice of Physic” (1768).

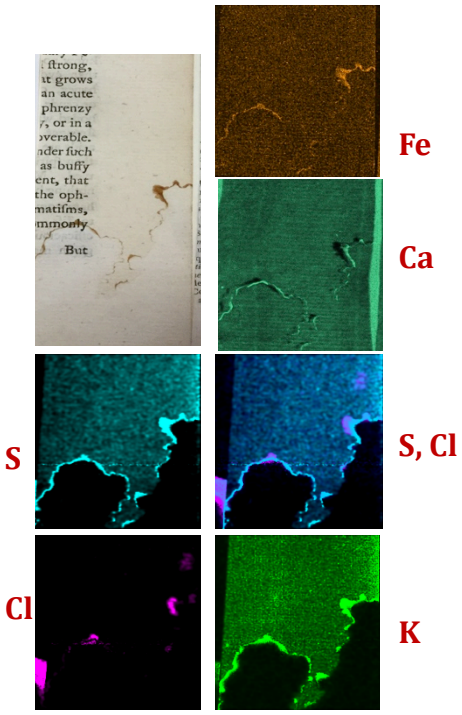
Fe
Ca
S
S, Cl
Cl
K

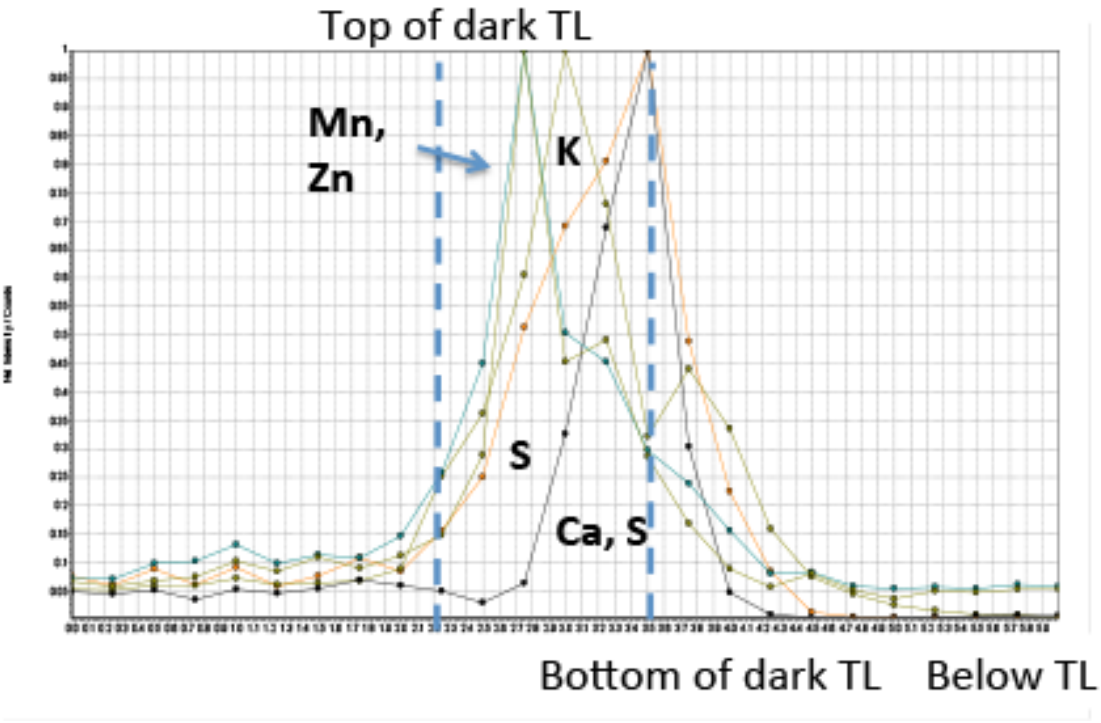
Top of dark TL
Mn,
Zn
K
S
Ca, S
Bottom of dark TL
Below TL

Figure 9. XRF maps acquired in model paper samples with tidelines: the top is an image of the sample set. The XRF maps below correspond, from top to bottom, to the following elements: S, Cl, S & Cl, K, Fe, Ca.
The order of paper samples, from left to right is as follows: UICB 2000, Test 11, Day 0; Whatman 1 Test 11 pre-aged, Day 0; Whatman 1 Test 10, Day 3.5; Whatman 1 Test 10, Day 1.5; Whatman 1 Test 10, Day 2.5; Lana 2 Test 11 pre-aged Day 0; Lana 3 Test 11, pre-aged, Day 3; UICB Ptolemy (unsized), Day 1.5; UICB Ptolemy (unsized) Day 3.5, UICB Ptolemy (unsized), Day 2.5; UICB 2000 Test 11 pre-aged Day 0.

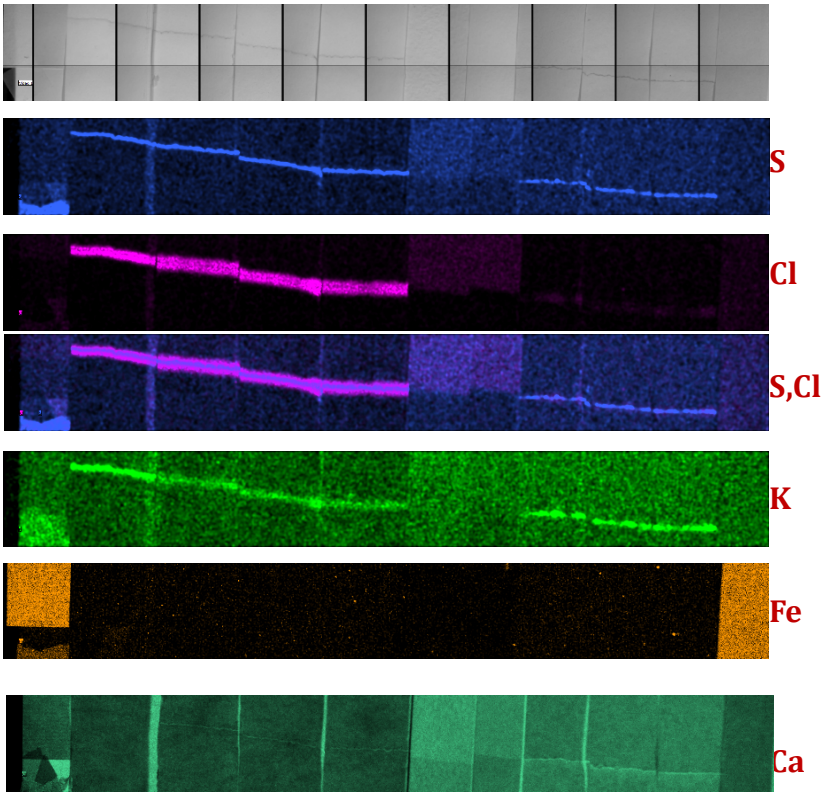

Figure 10. SXRF element maps of tideline region on Whatman 1 from Argonne.

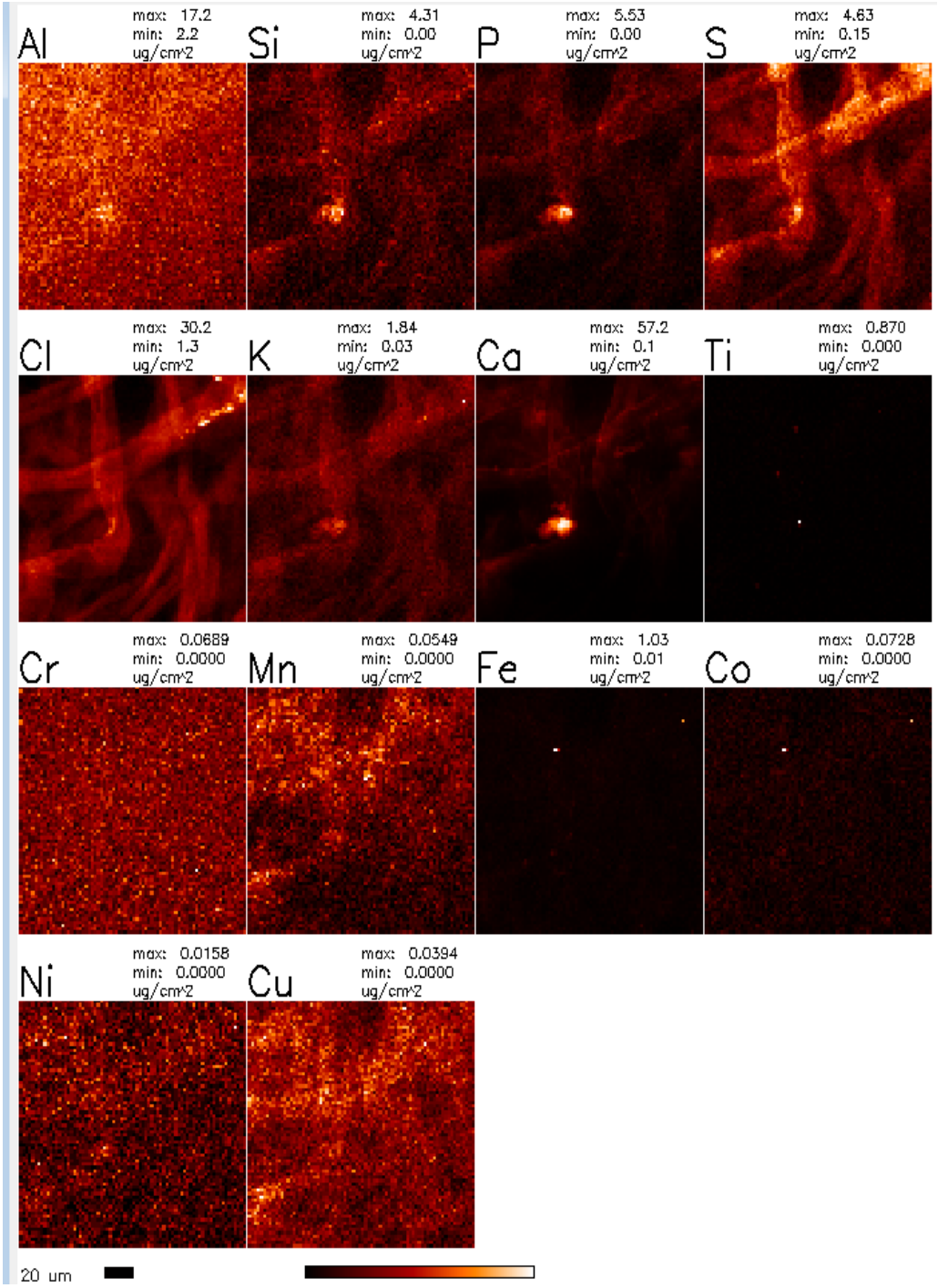

Figure 11. BSE image and EDS spectra from tideline area (EDS region shown in red) of Whatman 1 paper with laboratory-produced tideline (unaged).

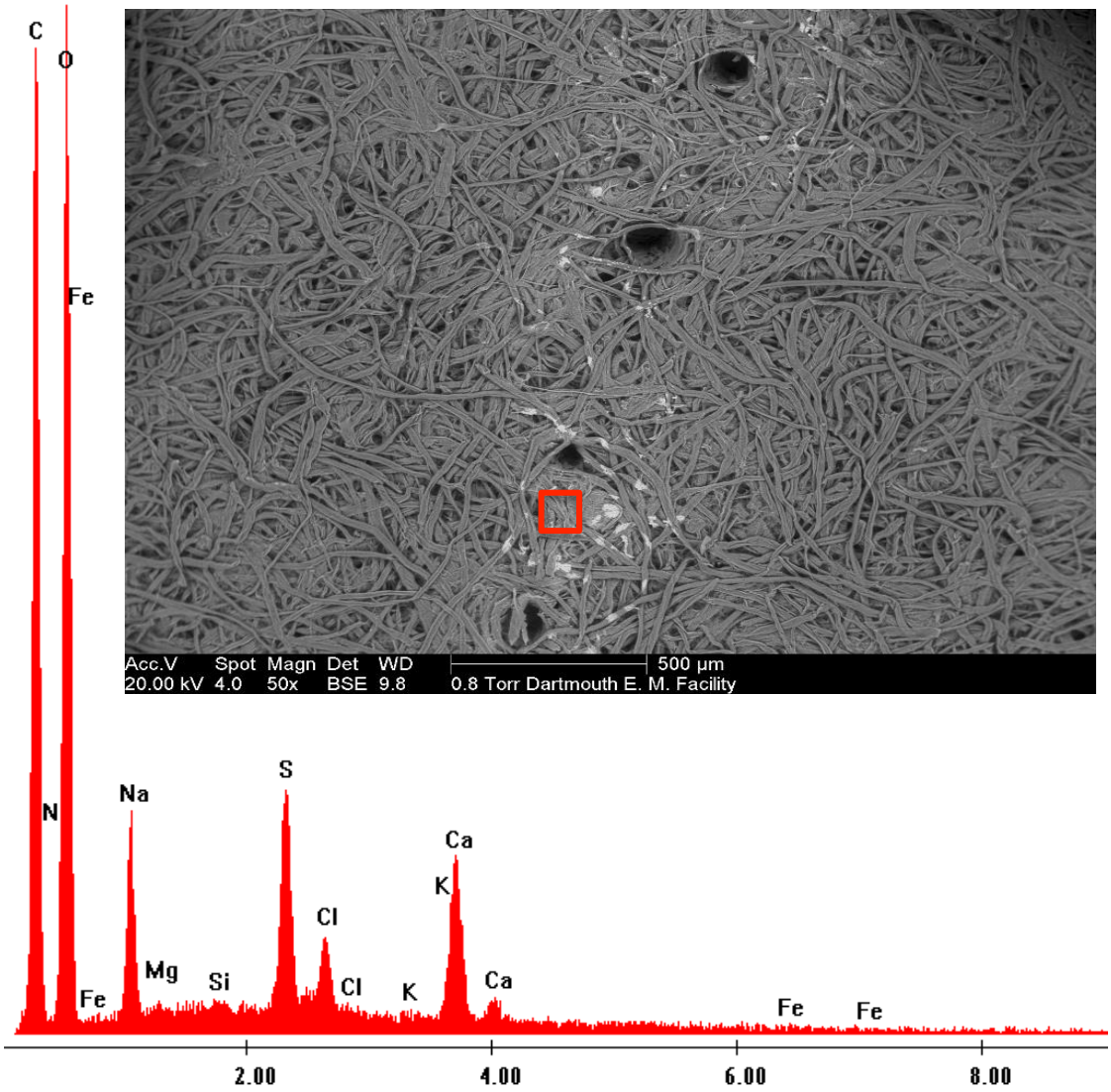

Figure 12. SEM/EDS of unsized UICB Ptolemy paper after 1.5 days artificial aging. EDS spectra from locationa above (top), on (middle) and below (bottom) the tideline (marked with holes).

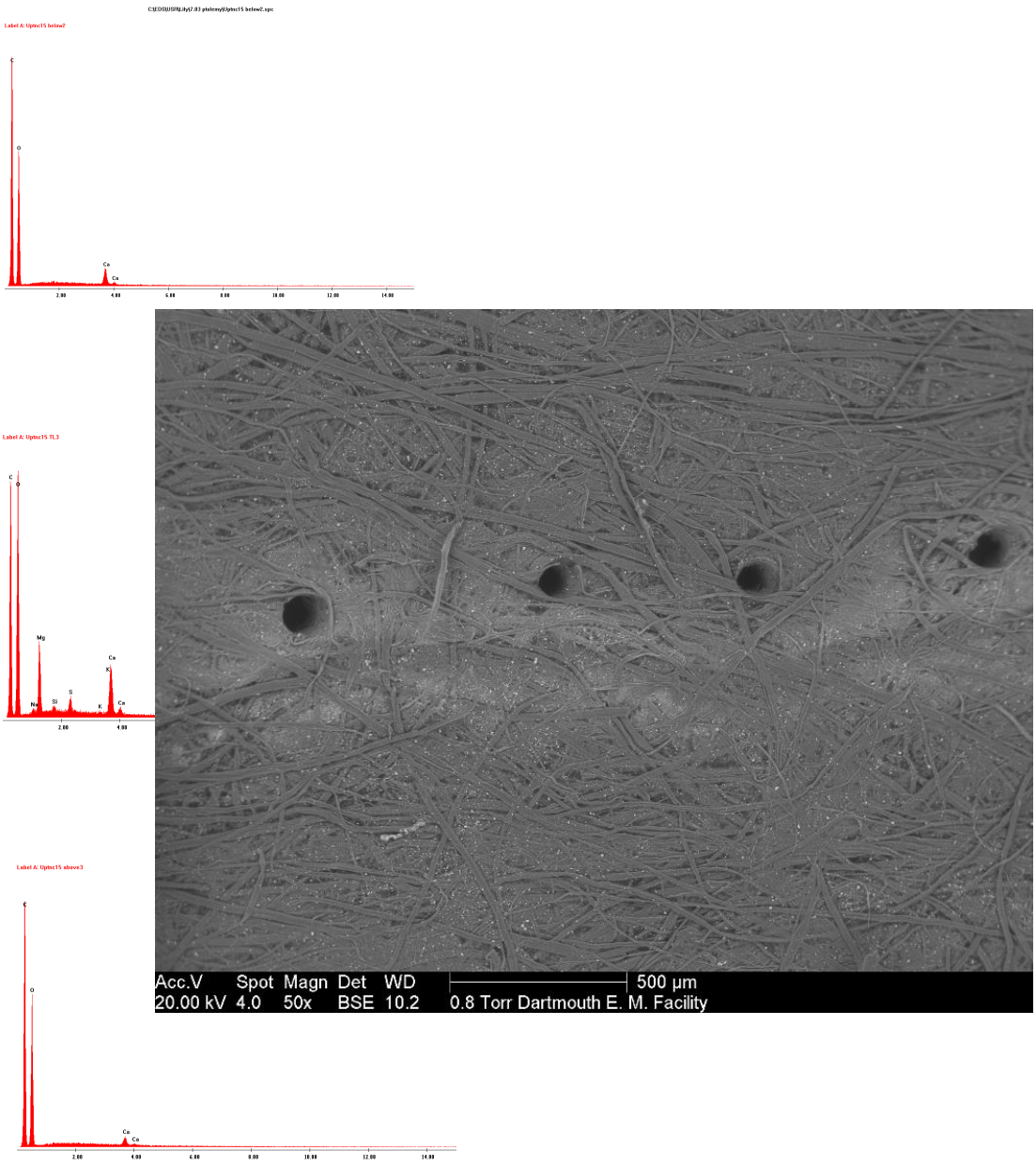

Figure 13. SEM BSE image of tideline region on Whatman 1 (top) and associated element maps (below) and combined false color map (left).

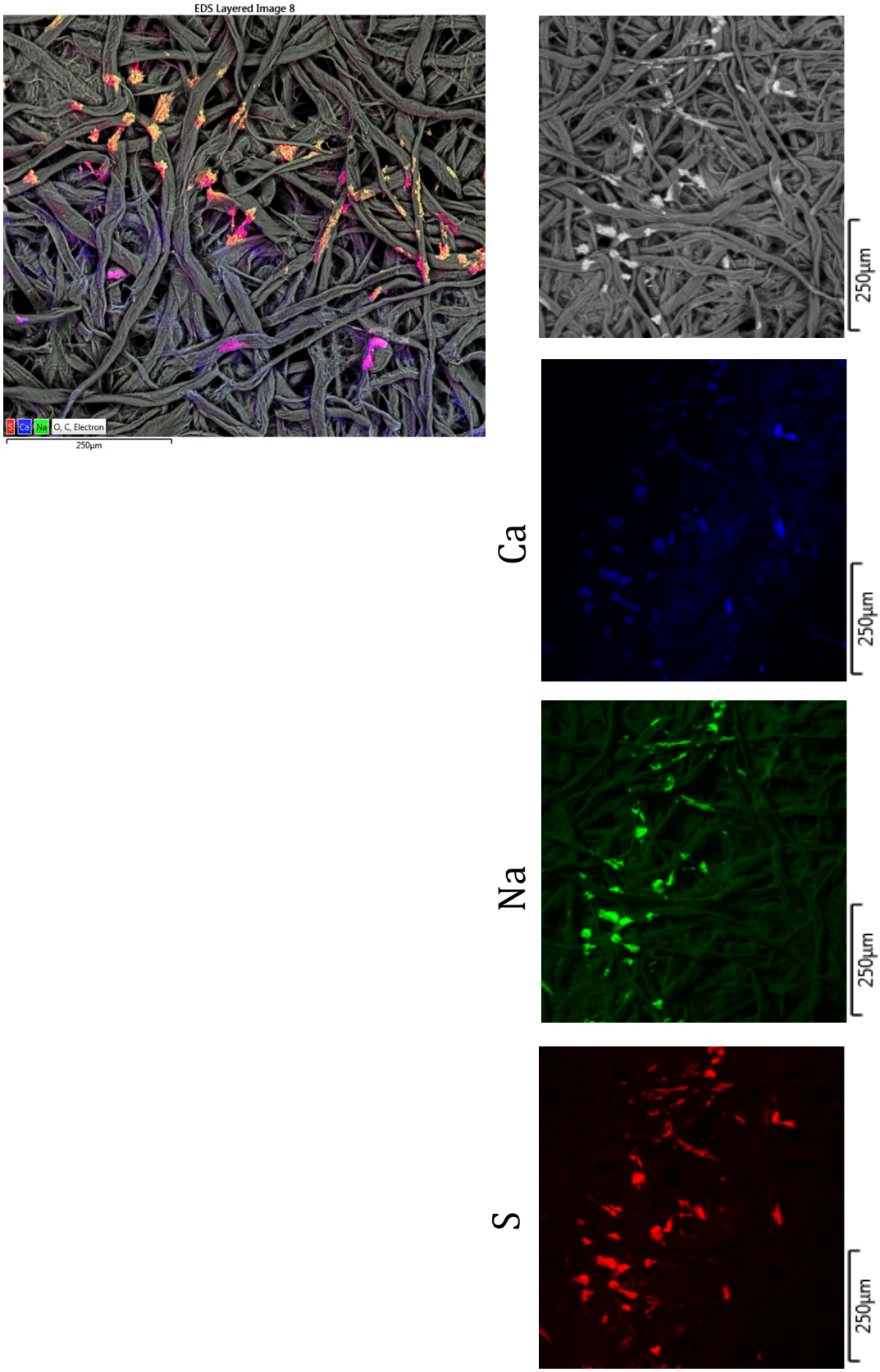

Figure 14. False color maps from tideline region on the UICB unsized paper, after 21 days of aging. The bottom right image combines the assigned colors showing how different elements deposit as particles and in bands and co-locate, e.g. Mg and S.

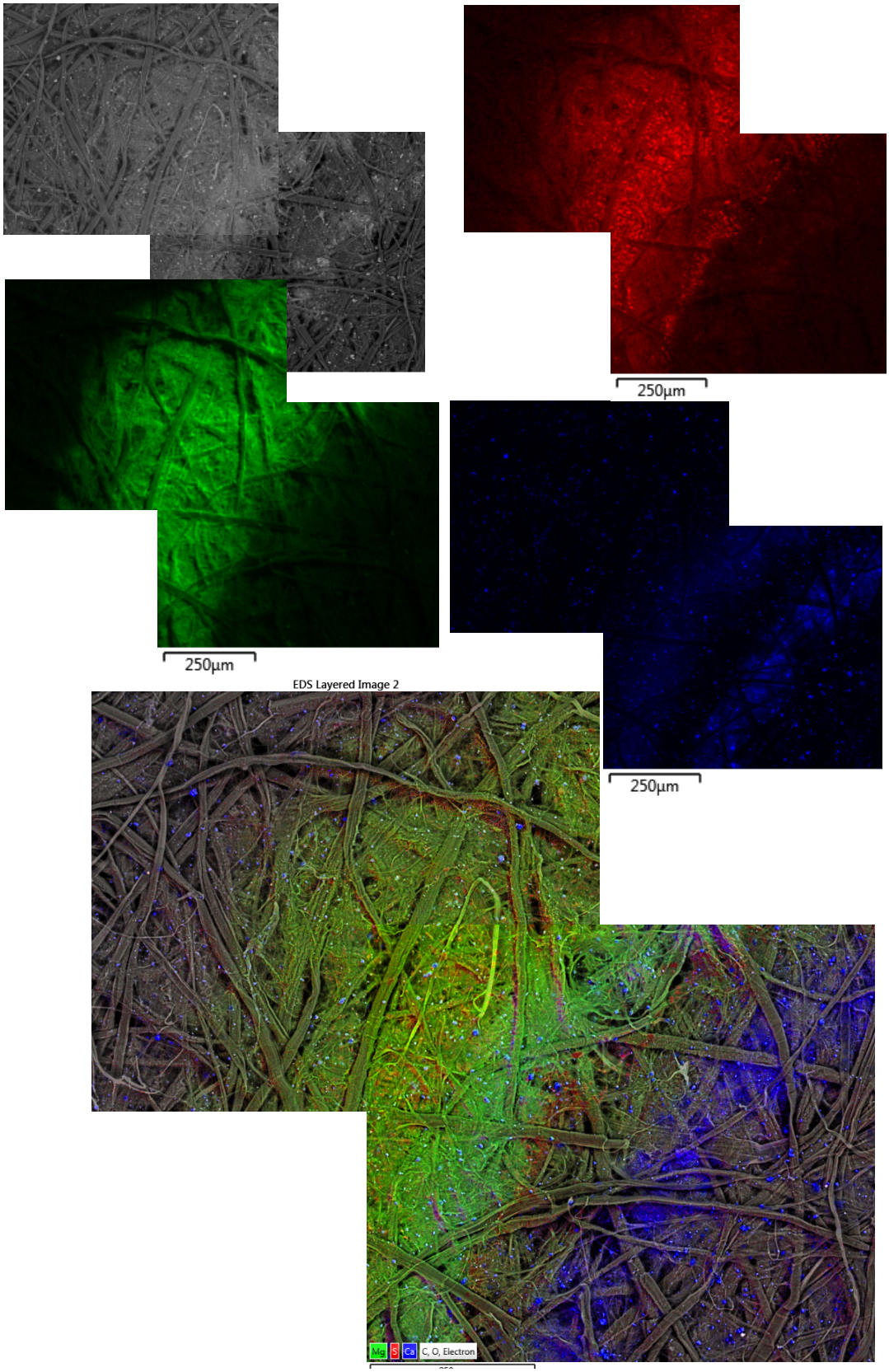

Figure 15. False color map of laboratory-made tideline on Barrow Book 1077.

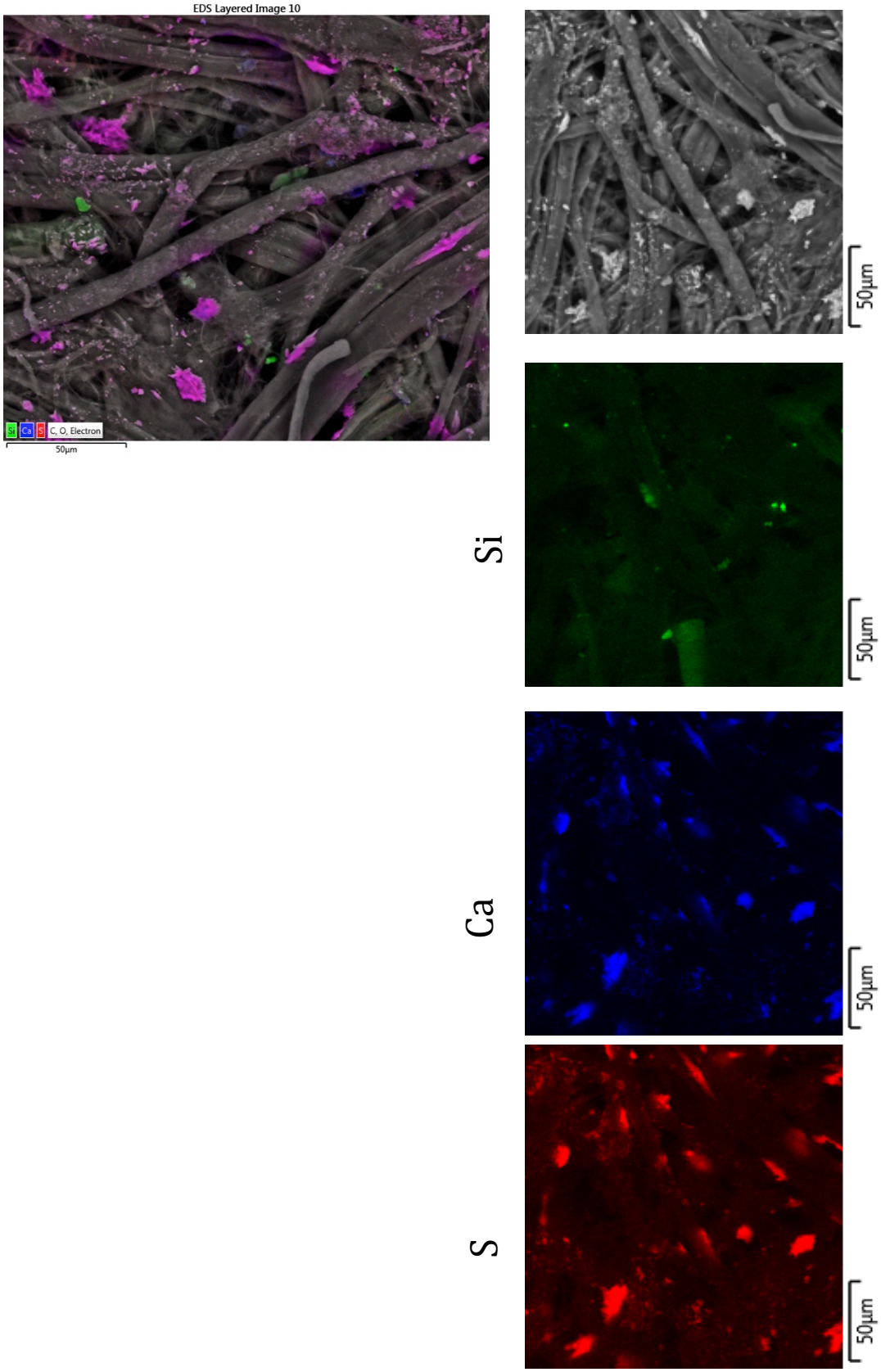

Figure 16. False color image of Whatman 1 from XRadia microCT analysis, produced with Osirix imaging software. The color on the tideline has been added for representational purposes. (Source: Teresa Porri)

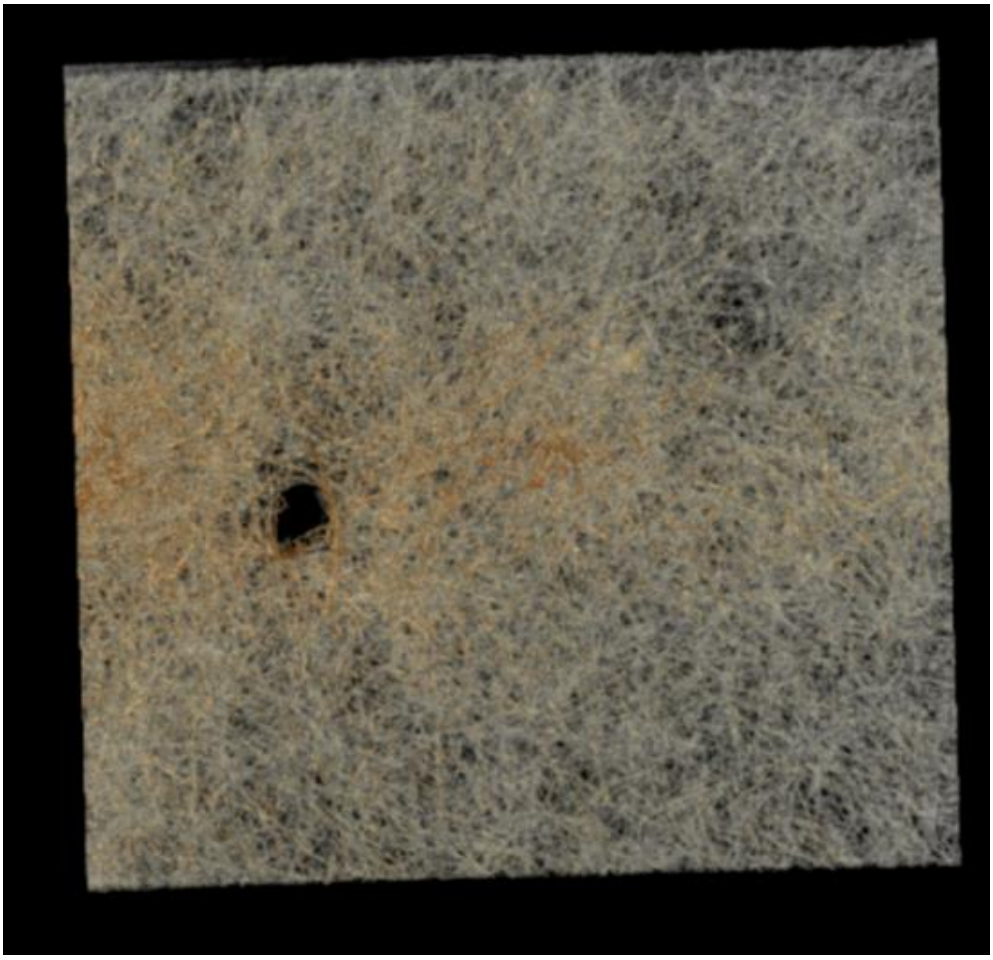

Figure 17. Orthogonal projections of Whatman 1 on 3D printed plastic sample holder. The hole marks the vertical height of the tideline.

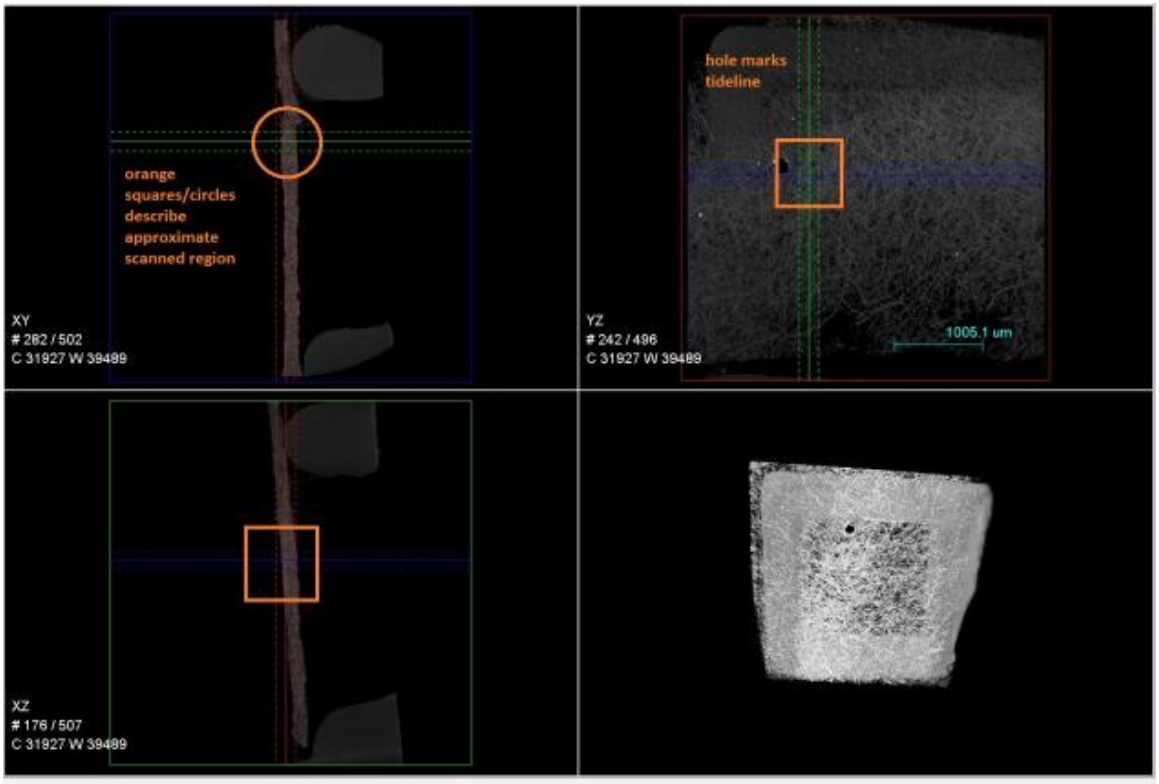

Figure 18. Whatman 1 microCT surface reconstruction (top) and multiorthogonal section (bottom) made with FEI Amira software.

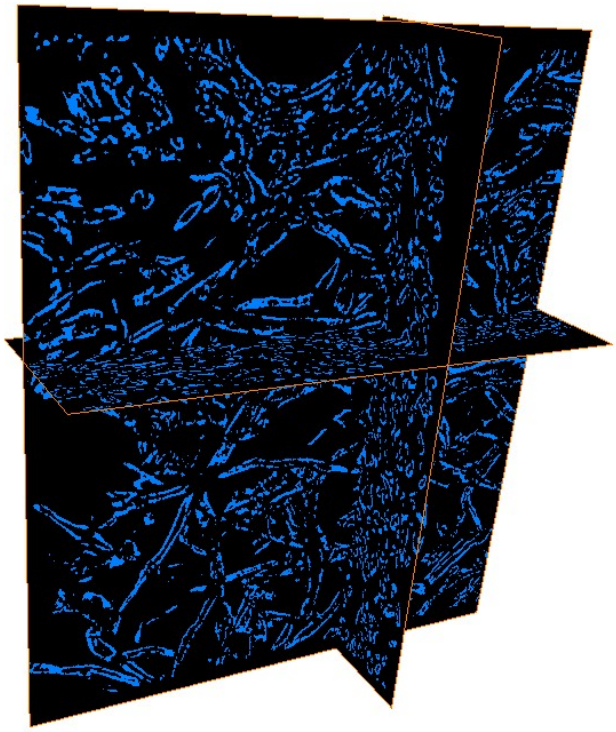
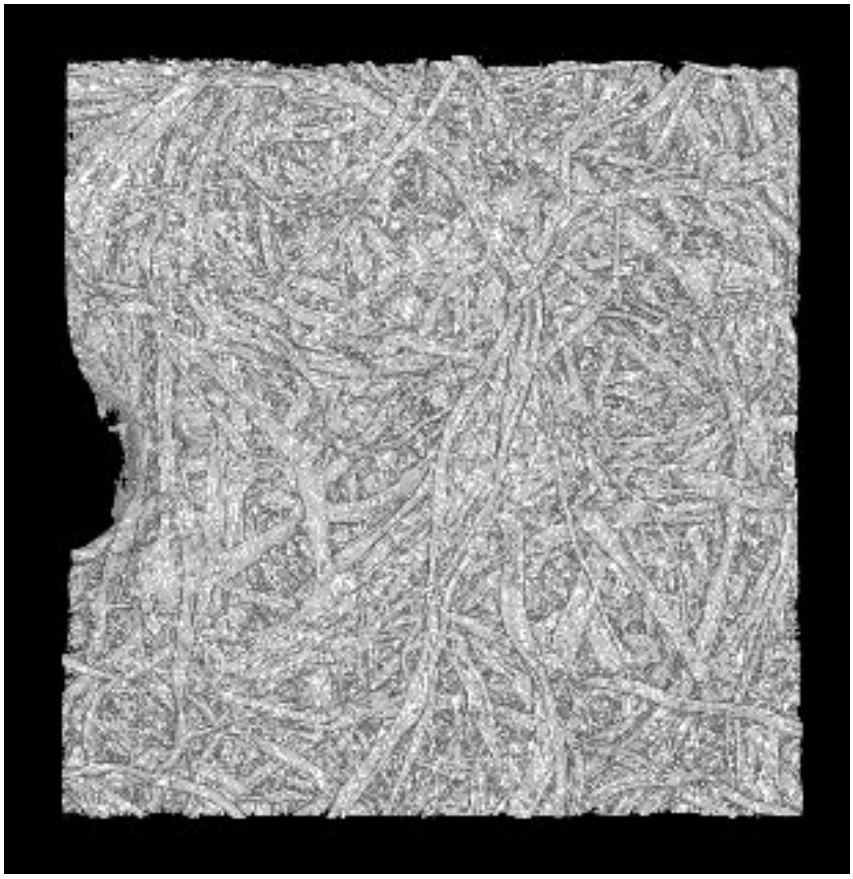
Figure 19. Image produced by FIJI 3D viewer